

An Informative Planning Framework for Target Tracking and Active Mapping in Dynamic Environments with ASVs

Sanjeev Ramkumar Sudha¹, Marija Popović², and Erlend M. Coates¹

Abstract—Mobile robot platforms are increasingly being used to automate information gathering tasks such as environmental monitoring. Efficient target tracking in dynamic environments is critical for applications such as search and rescue and pollutant cleanups. In this letter, we study active mapping of floating targets that drift due to environmental disturbances such as wind and currents. This is a challenging problem as it involves predicting both spatial and temporal variations in the map due to changing conditions. We propose an informative path planning framework to map an arbitrary number of moving targets with initially unknown positions in dynamic environments. A key component of our approach is a spatiotemporal prediction network that predicts target position distributions over time. We propose an adaptive planning objective for target tracking that leverages these predictions. Simulation experiments show that our proposed planning objective improves target tracking performance compared to existing methods that consider only entropy reduction as the planning objective. Finally, we validate our approach in field tests using an autonomous surface vehicle, showcasing its ability to track targets in real-world monitoring scenarios.

I. INTRODUCTION

Target search and monitoring with autonomous mobile robots has many applications, such as search and rescue [1], [2], cleaning pollutants [3], [4], and wildlife monitoring [5]. Mobile robot platforms such as autonomous surface vehicles (ASVs), and unmanned aerial vehicles (UAVs) allow for faster and more efficient search [6] compared to traditional approaches such as manned or teleoperated surveys [7] and static sensor networks [8]. For target tracking in *a priori* unknown dynamic environments, a robot must trade off between exploring previously unseen regions to discover new targets and acquiring new observations of previously observed moving targets to update their position estimates. Monitoring in such dynamic environments remains a challenging problem.

In this work, we consider the tracking of freely drifting targets with an ASV. We aim to build and maintain an accurate map of target positions in a dynamic environment for any number of targets with unknown initial positions. Partially submerged objects are subject to external disturbances such as waves, wind, and currents in the marine environment. This is a pertinent issue for maritime search and rescue [2], cleanups of plastic waste [3], or other pollutants [4].

¹Sanjeev R.S. and Erlend M. Coates are with the Department of ICT and Natural Sciences, Norwegian University of Science and Technology (NTNU), Norway. {sanjeev.k.r.sudha, erlend.coates}@ntnu.no

²Marija Popović is with the MAVLab, Department of Aerospace Engineering, TU Delft, The Netherlands. m.popovic@tudelft.nl

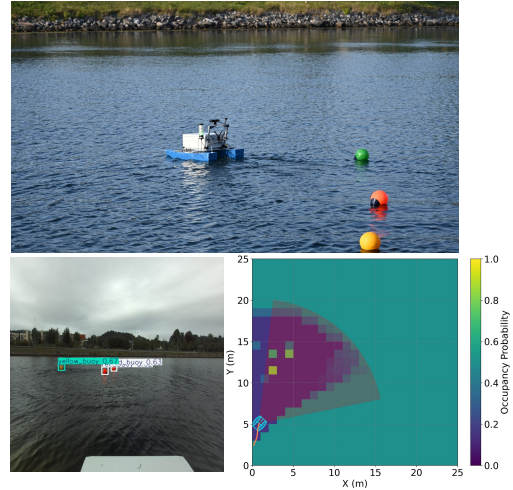


Fig. 1: Our informative path planning (IPP) framework applied to monitoring freely drifting targets (colored buoy markers) with an ASV that is equipped with a stereo camera. A dynamic mapping strategy is used for target tracking. We introduce a spatiotemporal prediction network and a new IPP objective that enable accurate target tracking.

Methods for finding sampling paths that maximize the information gathered for resource-constrained robots are termed *informative path planning* (IPP) [9]. Informative trajectories are quantified by an information-theoretic measure representing the mission objective, such as entropy in the map. For static environments, entropy is generally used as the planning objective for efficient spatial coverage [1], [10]. In dynamic environments, predicting spatial and temporal variations in the map over a certain time horizon is essential to plan informative trajectories for the robot. However, stochastic environmental disturbances such as wind and currents are hard to predict accurately for longer time frames.

Predicting changes in the environment is necessary to maintain an accurate map that represents the belief of target positions. Classical target tracking methods involve detecting, identifying, and estimating the velocities of multiple targets [11]. Using occupancy grid mapping for target tracking [12], [13] provides a simpler alternative by handling occupancy probabilities of the targets in a global probabilistic map representation. However, prior work [12]–[14] on occupancy grid mapping in dynamic environments learns state transitions through a series of observations, which is a challenging problem. If the dynamics governing the targets’

motion are known, they can be used to predict these changes.

To overcome these limitations, we present an IPP framework for actively mapping moving targets in dynamic environments. We introduce a spatiotemporal prediction network to predict future target position distributions, taking into account the uncertain drift due to stochastic environmental forces. This enables more efficient prediction of the uncertainty in target positions for longer time horizons and works for any number of targets. Furthermore, our proposed planning objective explicitly considers tracking of targets with uncertain position estimates using predictions from the network. A dynamic occupancy grid mapping approach is used to update the map with the sensor observations and an estimate of the targets’ drift using the measured wind velocity at each time step.

We make the following claims supported by extensive simulation experiments and field trials of our IPP framework implemented on an ASV: (i) our spatiotemporal network and the proposed IPP objective improve target tracking performance when compared to existing methods that use only entropy reduction as the planning objective, and (ii) incorporating drift predictions in the mapping stage improves mapping accuracy when compared to mapping without predictions. We open-source our software at https://github.com/sanjeevrs2000/ipp_dyntrack.

II. RELATED WORK

Target search is often formulated as an IPP problem [9]. Various studies have investigated IPP approaches for mapping discrete and static targets [1], [15]. Barrionuevo et al. [3] use reinforcement learning for planning to monitor and collect floating waste with a fleet of two ASVs, assuming perfect localization of the targets. Chen and Liu [16] study IPP for monitoring in dynamic environments with a model-predictive tree search with multi-objective optimization. They, however, assume that the environmental dynamics are deterministic, when in reality, long-term predictions are difficult due to the stochastic nature of real-life environments. Similar to [16], we use a sampling-based tree search algorithm for IPP that incorporates both the spatial and temporal variations in the map. In addition, our proposed spatiotemporal prediction network informs the informative planner of the uncertainties in target positions over the planning horizon, taking into account the stochastic nature of the wind and currents.

Some studies use high-fidelity numerical modeling of the underlying physical processes to guide adaptive sampling of oceanographic processes [17]–[19]. However, their adaptive planning strategies are limited to myopic behaviors, i.e. single-step lookahead, due to computational and operational constraints [17], [18]. Similar to these previous works, we use a learning-based spatiotemporal prediction model to inform the adaptive planning strategy. Our spatiotemporal network allows us to efficiently estimate the target position distributions over longer periods.

The occupancy grid mapping algorithm [20] is widely used in robotics to create probabilistic occupancy maps for static environments. Several studies extend the occupancy

grid formulation for mapping in dynamic environments, as relevant to our problem setup. Meyer et al. [14] propose a framework for mapping in dynamic environments where the state transition probabilities are learned. The Bayesian occupancy filter [12] introduces a dynamic occupancy grid mapping method for multi-object tracking. The map is updated in two steps, namely the estimation and prediction steps, similar to Bayesian state estimation. While our method is similar to that of Coue et al. [12], we infer the measured wind speed in the prediction at each time step rather than learning it through observations. It allows us to maintain a map that is agnostic to the number of targets while retaining the probabilistic formulation. This dynamic occupancy grid, combined with predictions from the spatiotemporal network, provides a framework to tackle the exploitation-exploration trade-off in dynamic environments.

Various recent studies apply deep learning-based methods for mapping temporally varying environments. Recurrent neural networks have been used to predict future occupancy states in dynamic environments [21], [22] in autonomous driving scenarios. Such methods rely on continuous observations of the targets of interest and predict the future dynamic states in the map for only a few seconds. Casado et al. [4] use a variational autoencoder to predict spatiotemporal pollutant distributions. Wang et al. [23] employ an attention-based neural network for persistent monitoring of mobile targets. In contrast to these works, we propose a physics-informed spatiotemporal prediction model that is independent of the number of targets and efficiently estimates uncertain target position distributions, for longer horizons of up to 30 s. Overall, our approach enables efficient tracking of moving targets with unknown initial positions in dynamic environments by providing an accurate map of target positions and predicting the changes in the map due to the dynamic environment. This enables effective autonomous monitoring for applications such as search and rescue and pollutant cleanups.

III. PROBLEM STATEMENT

Our aim is to detect and actively map targets of interest, such as floating waste, influenced by environmental disturbances in an *a priori* unknown environment. We frame this as an IPP problem [9]. We seek a trajectory \mathcal{T} from the set of all feasible trajectories Ψ , that maximizes an information-theoretic measure or utility $\mathcal{I}(\mathcal{T})$, given a limited budget B , such as mission time. In particular, the goal is to approximate the optimal trajectory \mathcal{T}^* given by

$$\mathcal{T}^* = \arg \max_{\mathcal{T} \in \Psi} \mathcal{I}(\mathcal{T}) \text{ s.t. } C(\mathcal{T}) \leq B, \quad (1)$$

where $C(\mathcal{T})$ is the cost associated with the trajectory \mathcal{T} .

IV. OUR APPROACH

A. Overview

We introduce a novel IPP framework for actively mapping moving targets in dynamic environments. An overview of our framework is shown in Fig. 2. We consider an ASV with a stereo camera for object detection and localization. A

probabilistic occupancy grid is used to map these detections. We also incorporate a prediction step in the mapping to compensate for the targets' drift. A key aspect of our approach is a spatiotemporal prediction network to estimate the spatial and temporal variations of the target positions over future time steps, given the current state of the occupancy grid and the current wind conditions. We then propose a new IPP utility formulation for target tracking that leverages predictions from our spatiotemporal network.

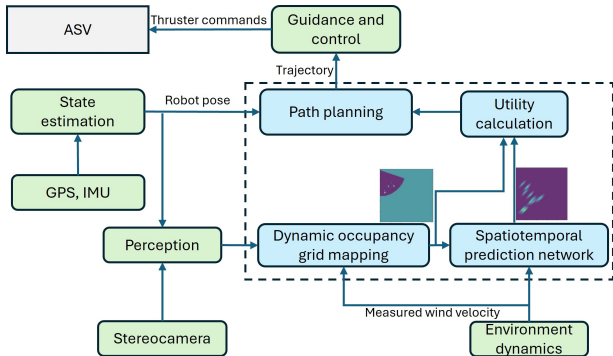


Fig. 2: An overview of our IPP framework (in blue) for active mapping of dynamic targets. We detect and localize targets with a stereo camera on an ASV. We use a dynamic occupancy grid mapping method that updates the map with both the sensor percepts and predicted motion of the targets. We introduce our spatiotemporal network that enables efficient predictions to aid the adaptive planning approach.

B. Perception

The ASV is equipped with a forward-facing stereo camera to detect and localize targets of interest. In this work, we use YOLOv8 [24] to identify the targets of interest, noting that our approach is agnostic to the choice of object detection algorithm. The positions of detected targets are projected onto the global occupancy map:

$$\mathbf{p}_g = \underbrace{\begin{bmatrix} c & -s & 0 \\ s & c & 0 \\ 0 & 0 & 1 \end{bmatrix}}_{R_{z\psi}} \underbrace{\begin{bmatrix} 0 & 0 & 1 \\ -1 & 0 & 0 \\ 0 & -1 & 0 \end{bmatrix}}_{R_{bc}} \mathbf{p}_c + \begin{bmatrix} x_v \\ y_v \\ 0 \end{bmatrix}, \quad (2)$$

where \mathbf{p}_c is the estimated depth of the target in the camera frame, \mathbf{p}_g is its position in the global east-north-up (ENU) frame. The rotation matrix for transformation from the camera to the body frame is denoted by R_{bc} , assuming the camera is forward-facing and the distance between the body's origin and the camera is negligible. The body to global frame rotation matrix is given by $R_{z\psi}$, where c and s denote $\cos \psi$ and $\sin \psi$. The estimated global position and heading of the ASV are denoted by (x_v, y_v) and ψ respectively.

Occupancy grid mapping requires inverse sensor models to convert sensor observations to belief probabilities on the map. To define inverse sensor models for our application, we perform an empirical analysis in simulations to estimate the localization error of the detected objects. The inverse

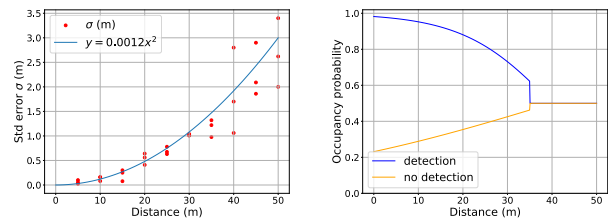


Fig. 3: Localization error $\sigma(r)$ as function of distance to detection r based on empirical analysis (left). The inverse sensor models used for mapping are shown on the right.

sensor models we use are similar to previous work [10], [25], but are kept asymmetric to better suit our problem setup in dynamic environments. Another distinction is that the inverse sensor model for detection also associates an occupancy probability for neighboring cells of each detection with a Gaussian kernel to take into account the localization errors in the detections. We derive the standard deviation $\sigma(r)$ of this error as a function of the distance to the detection r , through empirical analysis. To do this, we place a single object at various distances and relative heading angles to the camera in the simulation environment. We show the resulting standard deviations in the errors of the estimated positions of the targets in Fig. 3. We fit a curve over this plot to estimate the error as a function of the distance. Our inverse sensor models are defined as:

$$p(m_{i,j} | z) = \frac{1}{1 + e^{a(r-d)}} \cdot e^{-\frac{\|\mathbf{x}_c - \mathbf{x}_d\|^2}{2\sigma^2}} \quad (3)$$

$$p(m_{i,j} | z') = \frac{1}{1 + e^{a'(r-d')}} \quad (4)$$

where the standard deviation $\sigma(r)$ is set to $0.0012r^2$, based on the analysis in Fig. 3. The estimated position of the detected target is given by \mathbf{x}_d , and $\|\mathbf{x}_c - \mathbf{x}_d\|$ denotes the distance of a nearby cell c to this detection. The inverse sensor model associating a detection probability to cell (i, j) given a detection is denoted by $p(m_{i,j}|z)$, parameterized by a, d . The negative inverse sensor model for updating free cells is given by $p(m_{i,j}|z')$, parameterized by a', d' . The radial field of view is clipped at 35 m, as depth measurements become unreliable for further detections. The inverse observation models are depicted in Fig. 3.

C. Dynamic Occupancy Grid Mapping

We introduce a dynamic occupancy grid method for mapping, which is updated in two stages at each time step, namely the estimation and prediction steps. First, in the estimation step, the map is updated with the sensor observations, using the classical probabilistic occupancy grid algorithm [20]. In the prediction step, we compensate for the drift of targets in the map with the instantaneous wind speed. In the estimation step, we update the map recursively as:

$$l(m_{i,j}|z_{1:t}) = l(m_{i,j}|z_{1:t-1}) + l(m_{i,j}|z_t) - l(m_{i,j}), \quad (5)$$

where z_t is the sensor observation at time step t . The log odds nation of the occupancy state $p(m_{i,j} | z_{1:t})$ of a cell (i, j)

given the observations $z_{1:t}$ up to t , is denoted by $l(m_{i,j}|z_{1:t})$. The log odds representation of the inverse sensor model $p(m_{i,j}|z_t)$ is denoted by $l(m_{i,j}|z_t)$.

In the prediction step, the occupancy grid is updated each time step to account for the drift of the targets. We consider targets of interest such as floating waste on the water surface. For such objects, the wave effects are ignored as the drift due to the wind is more significant [26], [27]. We assume that the drift velocity can be approximated as being proportional to the instantaneous wind velocity, in line with previous work [26]. The drift for a single time step can therefore be approximated as:

$$\begin{aligned} dx &= \gamma v_w \cos(\psi_w) \Delta t, \\ dy &= \gamma v_w \sin(\psi_w) \Delta t, \end{aligned} \quad (6)$$

where v_w is the wind speed, ψ_w is the direction of the wind velocity at time t , and Δt is the time step between successive updates of the map. The wind factor γ is defined as the ratio of the drift speed of the object to the wind speed, which we set to be 0.03 following Rohrs et al. [26]. To update the occupancy grid with the drift prediction of the targets, we first filter it in order to keep only occupied cells (> 0.5) as:

$$m'_{i,j} = \begin{cases} m_{i,j}, & m_{i,j} > 0.5, \\ p_{\text{low}}, & \text{otherwise,} \end{cases} \quad (7)$$

where $m'_{i,j}$ denotes the occupancy probabilities in the filtered grid \mathcal{M}' . As the incremental drift at each time step is much smaller than the resolution of the occupancy grid, we store the accumulated drift in variables R_x, R_y . In the prediction step, the occupancy probabilities are updated only if $\text{round}(R_x) > 0$ or $\text{round}(R_y) > 0$. The update rule for the prediction step is described in lines 19-21 of Algorithm 1, where α and β are parameters to trade-off between the current occupancy state and the prediction. The occupancy probabilities in the grid are limited between $(p_{\text{low}}, p_{\text{high}}) = (0.15, 0.9)$ to adapt the mapping to the dynamic setting. A condensed form of this dynamic occupancy grid mapping algorithm is given in Algorithm 1.

D. Spatiotemporal Prediction Network

We introduce a spatiotemporal prediction network to predict the uncertainty of the target positions in the map over some time horizon. Although our dynamic occupancy grid mapping method contains a prediction step to estimate the drift of targets, it is not accurate at predicting drift for longer time horizons, due to the stochastic nature of environmental disturbances. Therefore, we first create a formulation to estimate the spatial and temporal variations of the target positions for future time steps.

We assume that the position of each target is represented by a Gaussian kernel, with the uncertainty in its position estimate growing with time, similar to previous work [23]. To reflect this assumption, we assume that the variances of the kernel are proportional to the wind speed and increase with the prediction time, with the principal axis being along the direction of the measured wind. We assume that the centers

Algorithm 1 Dynamic occupancy grid mapping

Ensure: Occupancy grid \mathcal{M}

- 1: Initialize $R_x \leftarrow 0, R_y \leftarrow 0, \mathcal{M} = 0.5$
- 2: **for** $t = 0 : B$ **do**
- 3: $O \leftarrow \phi$
- 4: **for** each detection d **do** ▷ Estimation step
- 5: Localize d at \mathbf{x}_d
- 6: Find cells c around d s.t. (3) $> p_{\text{low}}$
- 7: Update $m_{i,j}$ for all c with (3)
- 8: $O \leftarrow O \cup c$
- 9: **end for**
- 10: $F \leftarrow \text{fov}(\mathbf{x}^t) \setminus O$
- 11: **for** each $(i, j) \in F$ **do**
- 12: Update with (4)
- 13: **end for**
- 14: Get \mathcal{M}' according to (7) ▷ Prediction step
- 15: Compute drift (dx, dy) according to (6)
- 16: $R_x \leftarrow R_x + dx/\Delta_x, R_y \leftarrow R_y + dy/\Delta_y$
- 17: $s_x \leftarrow \text{round}(R_x), s_y \leftarrow \text{round}(R_y)$
- 18: $R_x \leftarrow R_x - s_x, R_y \leftarrow R_y - s_y$
- 19: **for** all cells $(i, j) \in \mathcal{M}$ **do**
- 20: **if** $m'_{i,j} \neq m'_{i-s_x, j-s_y}$ **then**
- 21: $m_{i,j} \leftarrow \alpha m'_{i-s_x, j-s_y} + \beta m_{i,j}$
- 22: **end if**
- 23: **end for**
- 24: **end for**

of each kernel translate by distances calculated as per (6). The variance along the direction of the wind is assumed to be greater, as for most realistic scenarios, the wind speed varies faster than the direction [28]. Based on this assumption, the standard deviations of the kernel along the major and minor axes, σ_{\parallel} , and σ_{\perp} for a prediction interval t are set as $\sigma_{\parallel} = 0.5 \gamma v_w t$, and $\sigma_{\perp} = 0.2 \gamma v_w t$ respectively. In case of negligible wind speeds ($v_w \approx 0$), $\sigma_{\parallel} = \sigma_{\perp} = 0.1 t$.

We train our spatiotemporal prediction network in a supervised fashion to obtain these predictions. The network enables us to get these predictions for multiple prediction steps for any number of targets in an efficient way. An illustration of this spatiotemporal prediction network is shown in Fig. 4. The input to the network is a filtered binary grid \mathcal{K} with the target positions, which is obtained as follows:

$$k_{i,j} = \begin{cases} 1, & m_{i,j} > 0.5, \\ 0, & \text{otherwise.} \end{cases} \quad (8)$$

We provide the wind parameters v_w, ψ_w , and the prediction interval as other inputs to the network. The network output is a grid of the same size with predicted position uncertainties of the targets at an arbitrary time step. We use a UNet architecture [29], which is widely used for image-to-image prediction tasks such as segmentation. The wind parameters and the prediction time are embedded into the latent space of the network.

To train our network, a synthetic dataset is created to simulate input conditions with different wind conditions,

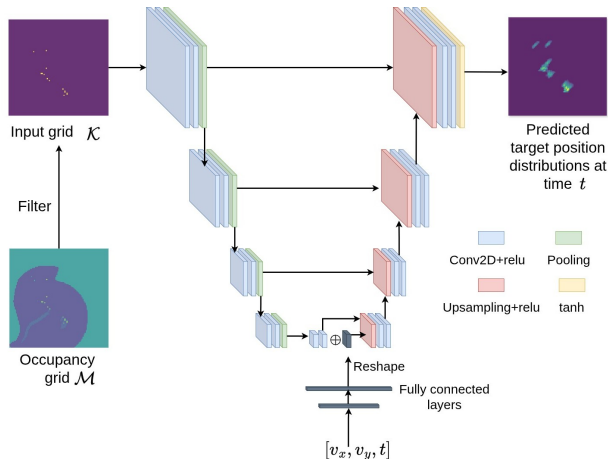


Fig. 4: An overview of our spatiotemporal prediction network. The inputs are a filtered grid with only target positions, along with a vector of the wind speeds v_x , v_y , and prediction interval t . The output is the predicted target position distributions at t .

target positions, and prediction intervals. To construct inputs resembling target occupancies in the map, binary grids of size 100×100 containing an arbitrary number of objects (< 20) with random positions are generated. For each of these input grids representing spatial distribution of the targets, outputs are computed as described above, for various combinations of wind parameters and prediction time steps. While predicting the drift of objects on the water surface is a difficult problem [27], we find that these assumptions suit our problem setup. Using an input representation that is agnostic to the number of targets makes our method generalizable, as validated through both simulation and field experiments, in Secs. V and VI.

E. Informative Planning for Dynamic Target Tracking

As the environment is dynamic, the robot needs to replan frequently to maintain an accurate map of target positions. The robot must explore unknown regions of the map while redetecting targets. Planning informative trajectories for the robot involves predicting both spatial and temporal variations in the environment. Commonly used IPP objectives are based on Shannon entropy measured based on the map state [10], [25]. However, these formulations do not explicitly account for temporal variations and periodic target redetections. In contrast, we exploit the predictions from our spatiotemporal network to include the temporal uncertainties in target positions in the planning objective.

To trade-off between exploring the environment and redetecting targets, we introduce a new planning utility that consists of both exploration and target tracking objectives. We propose a new target tracking component in the utility that explicitly considers possible target detections by estimating the spatiotemporal variations in the targets' position estimates in the planning objective. It is computed with the predictions from our spatiotemporal network, for prediction

steps over the considered planning horizon. To compute the predicted change in entropy, the dynamic occupancy grid mapping is forward-simulated for predicted measurements along considered trajectories. We define the planning utility as:

$$I(\mathcal{T}) = [H(\mathcal{M}|z_{\mathcal{T}}) - H(\mathcal{M})] + \frac{w}{|\mathcal{T}|} \sum_t J(\mathbf{x}^t), \quad (9)$$

$$J(\mathbf{x}^t) = \sum_{i,j} \frac{e^{-2 \cdot p_{ij}(t)}}{|\text{fov}(\mathbf{x}^t)|}, \quad \forall (i,j) \in \text{fov}(\mathbf{x}^t), \quad (10)$$

where $H(\mathcal{M})$ denotes the mean Shannon entropy of the occupancy grid, and $H(\mathcal{M}|z_{\mathcal{T}})$ denotes the predicted posterior mean entropy after simulating measurements $z_{\mathcal{T}}$ along a trajectory \mathcal{T} . The target tracking objective is defined as the averaged sum of the utility $J(\mathbf{x}^t)$ over the prediction steps, where \mathbf{x}^t is a pose on the trajectory corresponding to time t , and $p_{ij}(t)$ is the occupancy probability of cell (i,j) as output by our spatiotemporal prediction network. This explicitly considers tracking by rewarding possible detections with uncertain positions over the planning horizon. The weighting factor w determines the importance given to the two objectives, i.e., exploration and target tracking. In contrast to existing work [1], [25], our proposed target tracking utility promotes efficient target tracking by considering possible detections along the paths with the associated uncertain spatiotemporal variations in the target positions.

For planning, we use a sampling-based tree search to leverage these lookahead predictions. We consider a set of candidate paths Ψ constructed using a finite set of heading changes, assuming a constant speed for the ASV. These paths are further parameterized with Bézier curves to generate smooth and feasible paths for the ASV. The planning objective as described in (9)-(10), is calculated for each of these candidate paths \mathcal{T} .

V. RESULTS AND DISCUSSION

A. Experimental Setup

We perform simulations with an ASV in Gazebo with the VRX-simulator [30]. The wind is simulated as a stochastic process with the slowly varying component modeled as a first order Gauss-Markov process. We consider environments of size $100 \text{ m} \times 100 \text{ m}$ discretized with size $\Delta_x = 1 \text{ m}$, $\Delta_y = 1 \text{ m}$. We generate spherical buoy markers in the simulations as targets of interest and model the wind forces on these targets as described in Fossen [31]. Different scenarios are generated by changing the mean wind speed, mean direction, and the spawn positions of the targets. Eight targets are used in all scenarios, and the mean wind speed is varied between 6-10 m/s. We run Monte Carlo simulations under these environmental conditions to perform a statistical study of the different components of our framework.

We consider the following metrics for comparison: the mean Shannon entropy in the occupancy map \bar{H} , the mean squared error (MSE), and the mean detections (\bar{N}). The mean number of detections is computed as the average of the total number of detections, i.e., sum of the detections at each time

step. The MSE between the ground truth and the occupancy grid [3] is computed as:

$$\frac{\sum (\mathcal{M} - G \circledast \mathcal{Y})^2}{m \times n}, \quad (11)$$

where G is a Gaussian filter, \mathcal{Y} is the ground truth, \circledast is the convolution operator, m , n denote the height and width of the occupancy grid. The error is computed between the occupancy grid \mathcal{M} and $G \circledast \mathcal{Y}$ as \mathcal{Y} is a sparse matrix.

B. Ablation Study - Planning Utility

To study the effect of our spatiotemporal prediction network and the proposed planning utility, we compare various values of the weighting factor w in (9), which determines the trade-off between the two objectives: reducing entropy in the occupancy grid and redetecting targets. Monte Carlo simulations are performed for $w = 0, 2, 5$ and $5(1 - t/B)$, and the resulting metrics are shown in Table I. Higher values of w correspond to the planner prioritizing target redetection, while $w = 0$ corresponds to an exploratory planner that only considers the entropy reduction in the occupancy grid. The ASV speed is set to 1.5 m/s, and the planning horizon for the tree search is 25 s. Each Monte Carlo trial is run for $B = 250$ s.

w	H	\bar{N}	MSE
0	0.661 ± 0.015	1.123 ± 0.24	0.051 ± 0.008
2	0.688 ± 0.020	1.529 ± 0.132	0.065 ± 0.012
5	0.703 ± 0.027	1.56 ± 0.326	0.073 ± 0.016
$5(1 - t/B)$	0.681 ± 0.019	1.575 ± 0.24	0.061 ± 0.007

TABLE I: Comparative analysis for different values of w with the best values for each metric highlighted in bold. The trials with $w = 5(1 - t/B)$ are the best at target tracking, while the exploratory planner ($w = 0$) is the least effective.

Table I reveals that the purely exploratory case ($w = 0$) is the best at reducing entropy and MSE. It is also worse at detecting targets by up to $\approx 29\%$ as compared to the other variants that use the information from the prediction network into the planning objective. This highlights the importance of our prediction network and the corresponding target tracking utility in the adaptive planning strategy to re-identify targets. We see that the trials with $w = 5$ and $w = 5(1 - t/B)$ are nearly as effective at redetecting targets. These results demonstrate that our IPP utility improves target tracking performance by enabling more frequent target reacquisition.

C. Ablation Study - Mapping

To validate the advantages of our proposed prediction step of the dynamic occupancy grid mapping approach, we also perform simulation experiments without the prediction step of the mapping. Without the prediction step, the mapping is static and only relies on the sensor observations, as it does not account for any changes in the environment. We plot the resulting mapping accuracies and entropy for Monte Carlo simulations with and without the prediction step in Fig. 5.

The entropy values at the end of the mission are similar, i.e., 3.82% lower for the trials with the dynamic occupancy

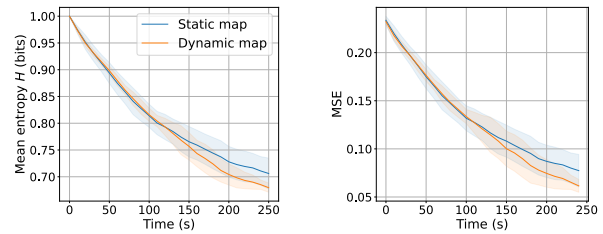


Fig. 5: Entropy and MSE for planning with the sampling-based planner, with and without the prediction step of the dynamic occupancy grid. The mapping accuracy is observed to be better by 21.8% with the prediction step.

grid mapping with the prediction step, as compared to mapping without the prediction step. However, the MSE values are 21.8% lower with our dynamic mapping approach as compared to the mapping without the prediction step. This indicates that the planner still effectively reduces uncertainty in the map in either case, as observed from the entropy. However, the mapping accuracy is better with the prediction step included, as the static occupancy grid does not account for the targets' motion. This could also lead to multiple detections of a single target on the map. Such errors in the mapping also subsequently influence the decision-making of the robot, leading to suboptimal planning.

D. Comparison With Baselines

We also evaluate our proposed sampling-based tree search planner by comparing it against other planning strategies. The factor w is adaptively changed as $5(1 - t/B)$. We choose the following baselines:

- 1) An implementation of the tree search in a receding horizon manner, executing a path with only three out of the five waypoints that are used to parameterize the Bézier path before replanning.
- 2) Greedy planner that greedily considers only a single waypoint to calculate utility (9).
- 3) Coverage planning with lawnmower motion, that is traditionally used for monitoring [32].
- 4) A random planner that selects waypoints randomly.

The coverage and random planners are non-adaptive strategies that do not take new information into account during the decision-making process. The computational burden of the replanning step prohibits implementation of a receding horizon planner where only the first waypoint is traversed before planning again. The replanning steps in case of the receding horizon and the sampling-based planners take 5 s for the considered horizon of 25 s and seven candidate paths, on a computer equipped with an i7-12700H processor and 32GB DDR5 RAM.

The mean entropy H , mean detections \bar{N} , and the MSE values for the various planning strategies are plotted in Fig. 6. We observe that the non-adaptive baselines perform the worst in exploring the map and also at redetecting targets. The greedy planner and the sampling-based planner report very similar scores in terms of entropy and MSE

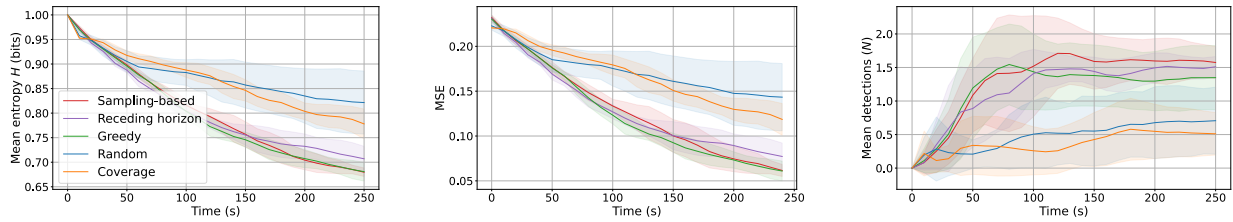


Fig. 6: Entropy, MSE, and the mean detections \bar{N} plotted with one standard deviation margin for the different planning strategies for the mission time (250 s). The proposed sampling-based planner is best at redetecting targets, closely followed by the receding horizon planner. Both these planning strategies benefit from longer lookahead predictions with the network. The greedy and sampling-based planners are both nearly as effective in reducing entropy.

measures, indicating they are equally effective at exploring the environment. However, the sampling-based planner is better at tracking targets, as it detects 16.8% more targets than the greedy planner, and 4.3% more targets as compared to the receding horizon planner at the end of mission time. This can be attributed to the sampling-based and receding horizon planners computing the utility by predicting sensor measurements along the path for the entire planning horizon, as opposed to the greedy planner, which greedily considers only the final waypoint on the path. From the entropy plot, we see that the receding horizon planner is not as effective in exploring the map as compared to the other adaptive strategies, due to the additional computational burden due to more frequent replanning, as the ASV has to stop and replan more frequently in this case.

VI. FIELD TESTS

To validate our framework in a real-world scenario, we perform field tests with an ASV for mapping freely drifting spherical floating buoy markers, as shown in Fig. 1. The ASV is overactuated with four thrusters in the X-configuration. It is equipped with a Cube Orange IMU and a Here4 GNSS for navigation. It has a Jetson Orin Nano, and software is implemented with ROS2 as middleware. Trials are performed on a $25\text{ m} \times 25\text{ m}$ area for a mission time of 150 s. We use a ZED 2i camera with 72° horizontal fov. We consider detections up to a distance of 15 m, as the camera gives reliable depth estimates up to 15-20 m. We use similar inverse sensor models for mapping as described in Sec. IV-B, with the parameters scaled accordingly. The ASV’s advance speed is set to 0.5 m/s, and the lookahead time for the planning step is 25 s.

During the experiments, moderate winds of 4 m/s were observed from West to East. We place four buoy markers near the left edge of the map at the start of each trial, and they are found to drift freely with the wind towards East due to the wind. We perform three trials with the sampling-based planner, each corresponding to $w = 0, 5$ and $5(1 - t/B)$, respectively, and discuss their results here. The resulting entropy and mean detections from the field trials are plotted in Fig. 7. It is observed that the trial with $w = 5$ is most effective at redetecting targets, as evident from several peaks in the graph for \bar{N} . These results align with simulations

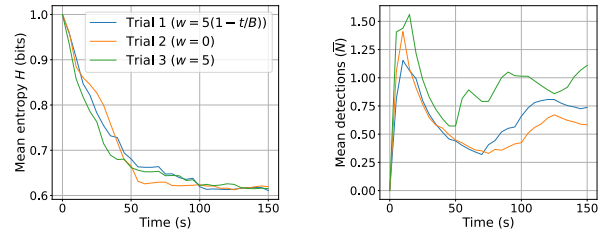


Fig. 7: Evolution of the mean entropy H and mean detections \bar{N} during our field trial missions. The trial with $w = 5$ is most effective at redetecting targets.

showing that higher values of w promote target tracking, further highlighting our proposed utility. We also show the occupancy maps at various instants for this trial in Fig. 8. The ASV first detects three of the four targets at $t = 15\text{ s}$. We notice that at later intervals, $t = 90\text{ s}$ and 145 s , the ASV tracks all four targets. An accompanying video of this experiment is also provided¹.

The field experiments are limited in that we do not have access to an anemometer to measure the wind velocity at each instant. Therefore, we assume the wind speed to be constant during the trials for the prediction step in the mapping. From Fig. 8, we see that the ASV can still track and redetect targets. This can be attributed to our IPP approach, which takes into account uncertain target positions with the help of the spatiotemporal network, enabling informative paths for target re-detection despite possible inaccuracies in the prediction step of the mapping.

VII. CONCLUSIONS AND FUTURE WORK

In this study, we introduce an IPP framework to actively map moving targets in dynamic environments. We introduce a spatiotemporal prediction network to estimate uncertain target position distributions over time due to drift, and a new IPP utility for target tracking. We use a dynamic occupancy mapping approach to maintain an accurate map. Simulation results show that our IPP approach with the proposed utility improves target tracking by redetecting targets more frequently, as compared to existing methods that use only

¹Video from the field trials with the ASV -<https://imgur.com/a/09aycaA>

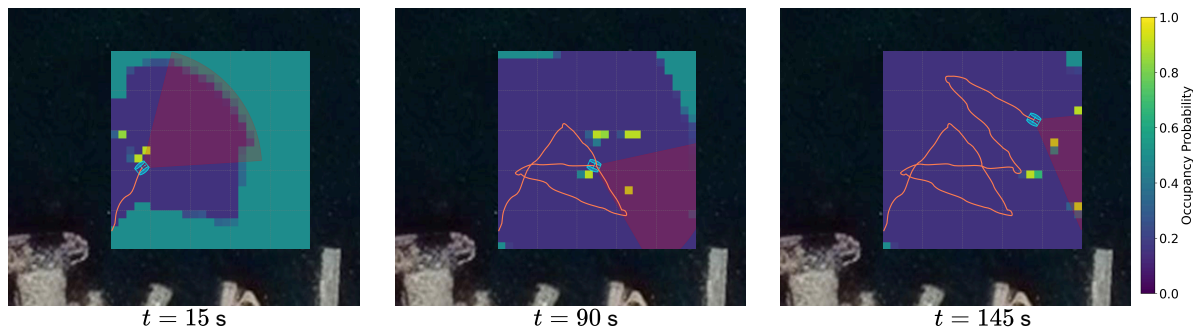


Fig. 8: Occupancy grids plotted at different time instants from the field trial. The path followed is given in orange, the ASV pose and its fov are given by the blue icon, and the red sector, respectively. At $t = 15$ s, the ASV has mapped three buoys, and at $t = 90$ s, it tracks the buoys again and has mapped all four buoys. The buoys are redetected again at $t = 145$ s.

entropy as the utility. The ablation studies further highlight the importance of our spatiotemporal network and our dynamic mapping method. Finally, field experiments with an ASV demonstrate our method's effectiveness in real-world monitoring scenarios. Although our proposed IPP approach performs well in both simulations and real experiments, the replanning step is computationally expensive, limiting the decision frequency. Future work will investigate learning-based techniques to develop efficient and faster IPP methods for monitoring in dynamic environments.

REFERENCES

- [1] A. A. Meera, M. Popović, A. Millane, and R. Siegwart, "Obstacle-aware adaptive informative path planning for uav-based target search," in *Proc. IEEE Intl. Conf. on Robot. & Automat. (ICRA)*, 2019.
- [2] B. Ai, B. Li, S. Gao, J. Xu, and H. Shang, "An intelligent decision algorithm for the generation of maritime search and rescue emergency response plans," *IEEE Access*, vol. 7, pp. 155 835–155 850, 2019.
- [3] A. M. Barrionuevo, S. Y. Luis, D. G. Reina, and S. L. T. Marín, "Optimizing plastic waste collection in water bodies using heterogeneous autonomous surface vehicles with deep reinforcement learning," *IEEE Robot. and Automat. Lett.*, 2025.
- [4] A. Casado-Pérez, S. Yanes, S. L. Toral, M. Perales-Esteve, and D. Gutiérrez-Reina, "Variational autoencoder for the prediction of oil contamination temporal evolution in water environments," *Sensors*, vol. 25, no. 6, p. 1654, 2025.
- [5] P. Tokekar, E. Branson, J. Vander Hook, and V. Isler, "Tracking aquatic invaders: Autonomous robots for monitoring invasive fish," *IEEE Robot. & Automat. Mag.*, vol. 20, no. 3, pp. 33–41, 2013.
- [6] M. Dunbabin and L. Marques, "Robots for environmental monitoring: Significant advancements and applications," *IEEE Robot. & Automat. Mag.*, vol. 19, no. 1, pp. 24–39, 2012.
- [7] R. R. Murphy, *Disaster robotics*. MIT press, 2017.
- [8] A. Lanzolla and M. Spadavecchia, "Wireless sensor networks for environmental monitoring," *Sensors*, vol. 21, no. 4, 2021.
- [9] M. Popović, J. Ott, J. Rückin, and M. J. Kochenderfer, "Learning-based methods for adaptive informative path planning," *Robot. and Auton. Sys.*, vol. 179, p. 104727, 2024.
- [10] M. Popović, T. Vidal-Calleja, G. Hitz, J. J. Chung, I. Sa, R. Siegwart, and J. Nieto, "An informative path planning framework for uav-based terrain monitoring," *Auton. Robots*, vol. 44, no. 6, pp. 889–911, 2020.
- [11] C. Robin and S. Lacroix, "Multi-robot target detection and tracking: taxonomy and survey," *Auton. Robots*, vol. 40, pp. 729–760, 2016.
- [12] C. Coué, C. Pradalier, C. Laugier, T. Fraichard, and P. Bessière, "Bayesian occupancy filtering for multitarget tracking: an automotive application," *Intl. Journal of Robot. Research (IJRR)*, vol. 25, no. 1, pp. 19–30, 2006.
- [13] Ö. Erkent, D. S. Gonzalez, A. Paigwar, and C. Laugier, "Gridtrack: Detection and tracking of multiple objects in dynamic occupancy grids," in *"Proc. Computer Vision Sys. (ICVS)"*, 2021.
- [14] D. Meyer-Delius, M. Beinhofer, and W. Burgard, "Occupancy grid models for robot mapping in changing environments," in *Proc. Conf. on Advancements of Artificial Intelligence (AAAI)*, 2012.
- [15] A. Vashisth, J. Ruckin, F. Magistri, C. Stachniss, and M. Popovic, "Deep reinforcement learning with dynamic graphs for adaptive informative path planning," *IEEE Robot. and Automat. Lett.*, 2024.
- [16] W. Chen and L. Liu, "Multi-objective and model-predictive tree search for spatiotemporal informative planning," in *Proc. Conf. on Decision Making and Control (CDC)*, 2019.
- [17] V. L. Preston, G. E. Flaspohler, J. W. Fisher, A. P. Michel, and N. Roy, "Phortex: Physically-informed operational robotic trajectories for scientific expeditions," *IEEE Trans. on Field Robotics*, 2024.
- [18] M. O. Berild, Y. Ge, J. Eidsvik, G.-A. Fuglstad, and I. Ellingsen, "Efficient 3d real-time adaptive auv sampling of a river plume front," *Frontiers in Marine Science*, vol. 10, p. 1319719, 2024.
- [19] S. Ma, C. Liu, C. M. Harvey, R. Bucknall, and Y. Liu, "Adaptive informative path planning for active reconstruction of spatio-temporal water pollution dispersion using unmanned surface vehicles," *Applied Ocean Research*, vol. 156, p. 104458, 2025.
- [20] A. Elfes, "Using occupancy grids for mobile robot perception and navigation," *Computer*, vol. 22, no. 6, pp. 46–57, 1989.
- [21] K. S. Mann, A. Tomy, A. Paigwar, A. Renzaglia, and C. Laugier, "Predicting future occupancy grids in dynamic environment with spatio-temporal learning," in *Proc. IEEE Intell. Veh. Symp. (IV)*, 2022.
- [22] M. Toyungyernsub, M. Itkina, R. Senanayake, and M. J. Kochenderfer, "Double-prong convlstm for spatiotemporal occupancy prediction in dynamic environments," in *Proc. IEEE Intl. Conf. on Robot. & Automat. (ICRA)*, 2021.
- [23] Y. Wang, Y. Wang, Y. Cao, and G. Sartoretti, "Spatio-temporal attention network for persistent monitoring of multiple mobile targets," in *Proc. IEEE/RSJ Intl. Conf. on Intell. Robots and Sys. (IROS)*, 2023.
- [24] G. Jocher, A. Chaurasia, and J. Qiu, "Ultralytics yolov8," 2023. [Online]. Available: <https://github.com/ultralytics/ultralytics>
- [25] B. Moon, S. Chatterjee, and S. Scherer, "Tigris: An informed sampling-based algorithm for informative path planning," in *Proc. IEEE/RSJ Intl. Conf. on Intell. Robots and Sys. (IROS)*, 2022.
- [26] J. Röhrs and K. H. Christensen, "Drift in the uppermost part of the ocean," *Geophysical Research Lett.*, vol. 42, no. 23, pp. 10–349, 2015.
- [27] Ø. Breivik, A. A. Allen, C. Maisondieu, and J. C. Roth, "Wind-induced drift of objects at sea: The leeway field method," *Applied Ocean Research*, vol. 33, no. 2, pp. 100–109, 2011.
- [28] J. C. Kaimal and J. J. Finnigan, *Atmospheric boundary layer flows: their structure and measurement*. Oxford university press, 1994.
- [29] O. Ronneberger, P. Fischer, and T. Brox, "U-net: Convolutional networks for biomedical image segmentation," in *Proc. of Image Computing and Computer-Assisted Intervention (MICCAI)*, 2015.
- [30] B. Bingham, C. Agüero, M. McCarrin, J. Klamo, J. Malia, K. Allen, T. Lum, M. Rawson, and R. Waqar, "Toward maritime robotic simulation in gazebo," in *Proc. MTS/IEEE OCEANS SEATTLE*, 2019.
- [31] T. I. Fossen, *Handbook of marine craft hydrodynamics and motion control*. John Wiley & Sons, 2011.
- [32] E. Galceran and M. Carreras, "A survey on coverage path planning for robotics," *Robot. and Auton. Sys.*, vol. 61, no. 12, pp. 1258–1276, 2013.